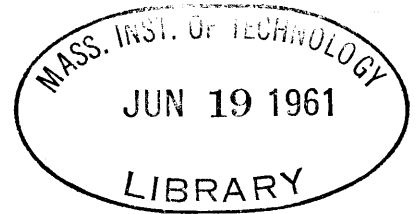# MAGNETIC REFLECTION OF A SHOCK-PRODUCED PLASMA

by

GERALD LOOMIS WILSON

Submitted in Partial Fulfillment

of the Requirements for the

Degree of Bachelor of Science

at the

MASSACHUSETTS INSTITUTE OF TECHNOLOGY

Signature of Author. . . . .
Department of Electrical Engineering, May 20, 1961

Certified by . . . .
Thesis Supervisor

Accepted by . . . .
Chairman, Departmental Committee on Theses

ABSTRACT

An experimental investigation is made of the interaction of a hydrogen plasma with the magnetic field of a solenoidal coil. Both reflected shocks and channelling phenomena are studied. Smear camera measurements of the reflected shock and channelling effect indicate that as the plasma enters the field region, the conductivity increases.

ACKNOWLEDGEMENTS

The author wishes to express his appreciation to Professor Herbert H. Woodson for suggesting this problem, for his advice and interest during the progress of the work and for his encouragement during the discouraging moments of experimentation.

The author also wishes to express his appreciation to Mr. Arthur Lewis for his helpful suggestions, and to Mr. Harold Atlas, Mr. Joseph Crowley, and Mr. James Thompson for their aid in the experimental part of the work.

I would also like to thank my wife Marian for typing the thesis.

TABLE OF CONTENTS

TABLE OF FIGURES

INTRODUCTION

Background

In recent years much effort has been devoted to the production of electrical energy through the media of fluids in motion under the influence of magnetic fields. The major drawback in most schemes has been the low conductivity to density ratios of any liquids, including mercury and sodium. In order to obtain ratios high enough to make a device feasible, highly ionized, seeded plasmas can be used. Also the low density of a gas as compared to that of a conducting liquid, suggests many applications in situations where weight is an important factor.

One method of converting the kinetic energy of a plasma, is to pass pulses of the gas through the center of a coil. As the gas passes through, the flux of the coil changes, and induces a voltage. This phenomenon can be utilized to build a parametric generator.

Objectives

In order to build such a device, the interaction of the gas with the magnetic field must be understood. Some theoretical analyses of an ionized gas impinging on a magnetic field discontinuity, have been done.[1, 2, 3] All of these analyses assume the gas to have infinite conductivity and the magnetic field to be a uniform field purly transverse to the direction of flow. In the device we are describing, the field has components both parallel and transverse to the flow, which cause the gas to be compressed and a shock to be reflected by the field

discontinuity. Furthermore, the infinite conductivity assumption is unrealistic when considering an energy conversion device. A realistic theoretical prediction of the interaction is therefore complicated.

The main objective of this experiment is to study the reflection of a shock, but some experimental data concerned with the compression of the plasma are also presented.

Description of Experiment

The geometry used is shown in Fig. 1. A coaxial driver is used to drive the plasma into a 51 mm cylindrical pyrex tube. The shock is formed by discharging ten parallel .25 microfarad capacitors, charged to 24 kv, across the inner and outer conductors of the driver. The trigger circuit for the shock tube is described by A. T. Lewis[4] in a summary of shock tube research. The shock passes through a solenoidal coil which has a pickup coil wound around the tube parallel to the field coil. High current pulse circuitry which is described in Appendix A, excites the field coil with a pulse whose length is long enough to create a magnetic field which looks essentially constant to the plasma.

Initially, velocity measurements were made with photomultipliers placed a known distance apart along the tube. Velocity measurements have since been improved upon through the construction of a rotating mirror camera. A description of the smear camera and associated instrumentation appears in Appendix B. Velocity measurements were made by placing a longitudinal slit along the direction of flow. The

FIELD COIL

PICKUP COIL

50 MM.

DRIVER
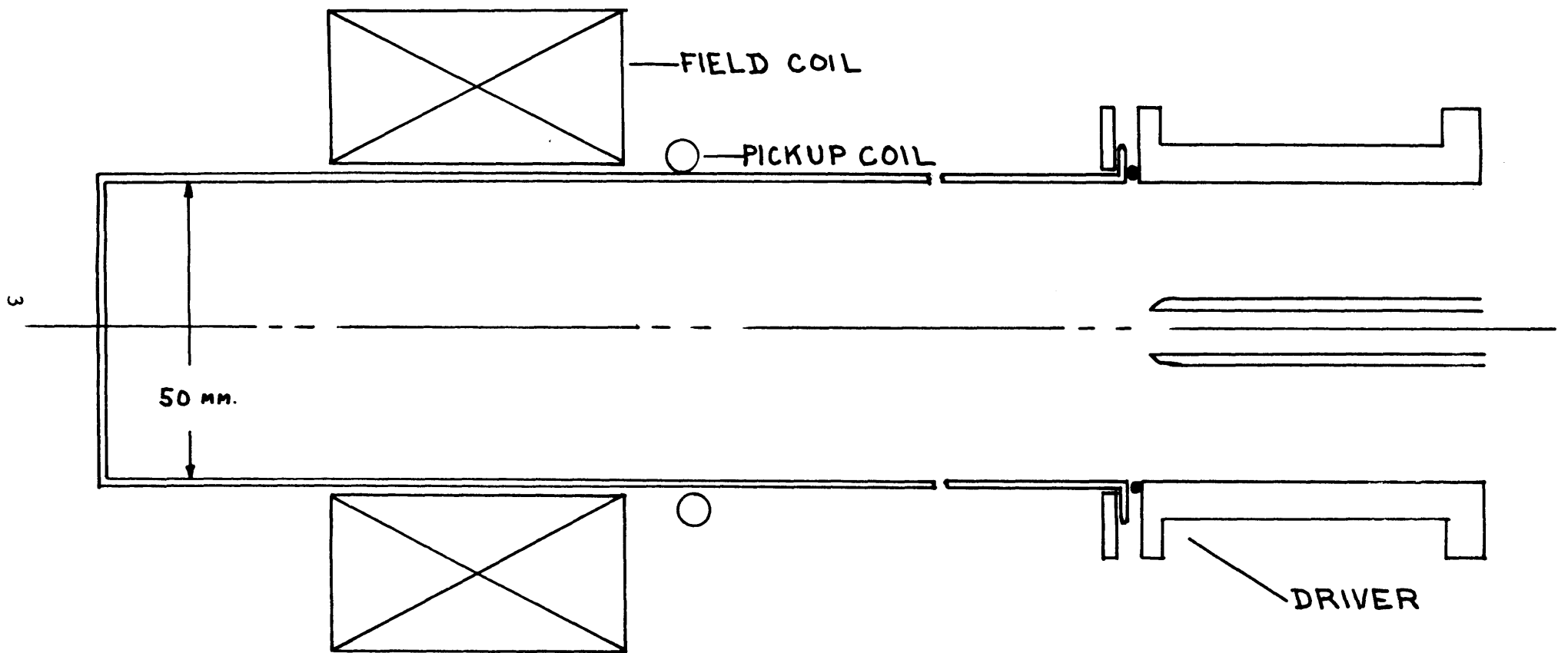
SHOCK TUBE GEOMETRY

FIG. 1

shock front is observed as a discontinuity in light, produced by recombination in the gas behind the shock as it moves down the tube. Smear camera pictures are also made through a slit transverse to the flow direction. The slit is placed 1 cm upstream from the field coil so that the channelling effect can be observed.

The procedure used for making one shock measurement is as follows.

With smear camera rotating at desired speed:

1. Pump system down to 1 micron of Hg. Close pump off.

2. Inject hydrogen through liquid air cold trap into shock tube until desired initial pressure is reached.

3. Charge capacitors in magnetic field system and then charge shock tube capacitors.

4. Switch off all lights and fire system.

Although measurements are made at many different initial pressures and discharge voltages, a description of the resulting shock wave produced under a given set of conditions, is presented so that the reader may become aquainted with the parameters involved. All measurements are made in hydrogen.

Initial pressure	.1 mm Hg
Discharge voltage	24 kv
Velocity measured at driver	9.5 cm/μs
Mach Number	72
Conductivity	2.25 $\times$ 10^4 mhos/meter
Temperature	69 $\times$ 10^3 °K
Magnetic Reynold's number	62

DESCRIPTION OF INTERACTION

Reflected Shock Discussion

Consider a slug of ionized gas moving into a solenoidal field coil. As shown in Fig. 2, the velocity of the gas combined with the radial compoent of the B field induces an azimuthal current in the gas as

$$\underline{J}_\theta = \sigma(\underline{E} + \underline{V} \times \underline{B}) = -\sigma V B_r \underline{i}_\theta \tag{1}$$

The $\underline{J} \times B$ forces produced by this induced current and the magnetic field have two effects on the gas.

$$\underline{J}_\theta \times \underline{B} = -\sigma V B_r^2 \underline{i}_z - \sigma V B_r B_t \underline{i}_r \tag{2}$$

The first expression is a force which opposes the motion of the oncoming gas. The forces in the radial direction channel the gas into a smaller cross section as the gas approaches the center of the coil. These combined phenomena are strongly coupled through changes in the parameters of the gas.

The curves of Fig. 3 show the ratio of the radial field to the maximum field at the coil center, plotted for different radial positions as a function of the axial distance from the center of the coil. It is apparent that an incoming slug of gas can never be reflected from a distance less than the axial position at which the radial field is a maximum. Secondly, if channelling is neglected, and gas conductivity is constant, the gas reflects from a distance further away from the center of the coil as the applied field is raised. This is done in such a manner as to keep the radial force term in Eq. 2 constant, and therefore
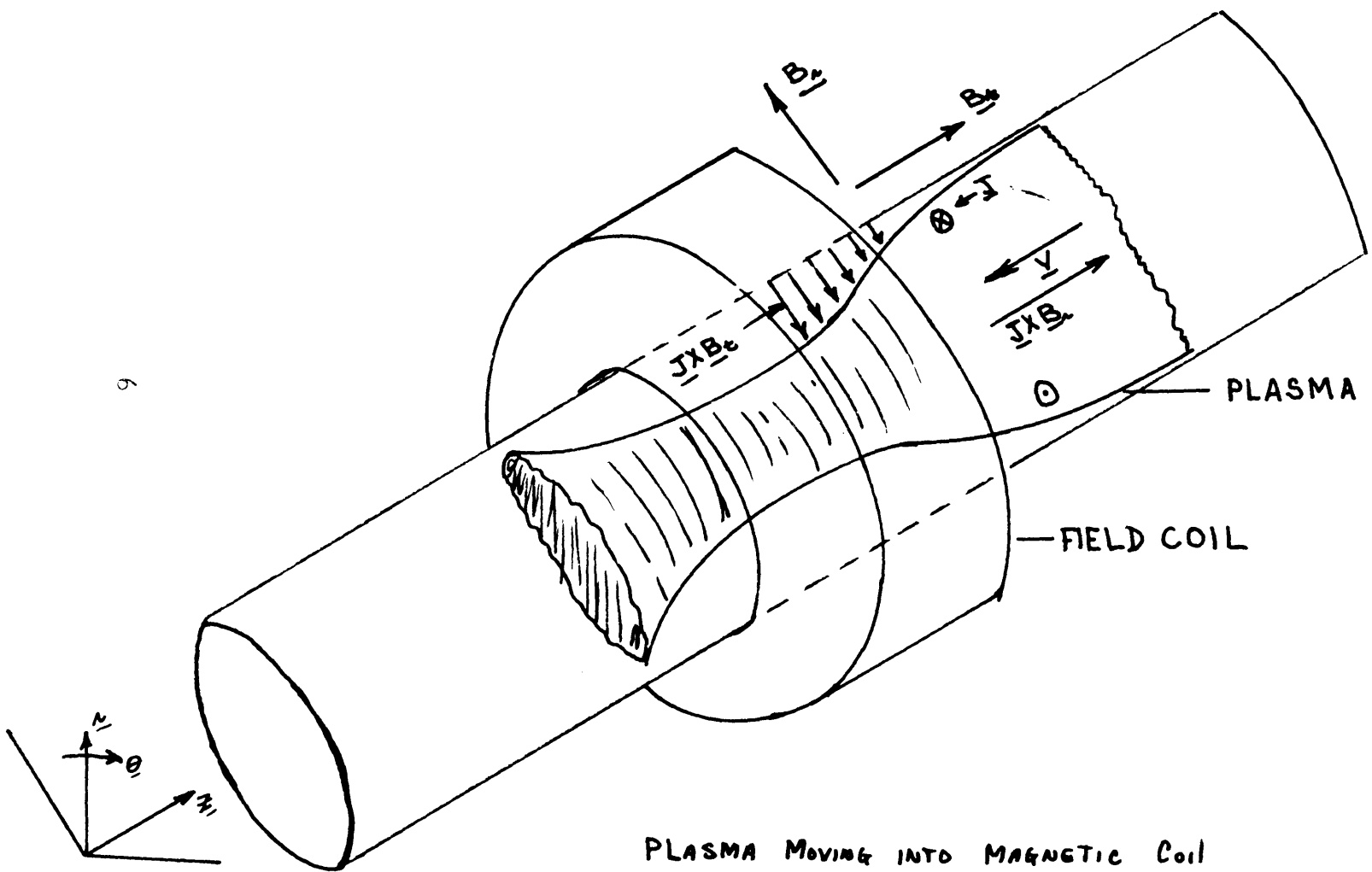
PLASMA MOVING INTO MAGNETIC COIL

Fig. 2

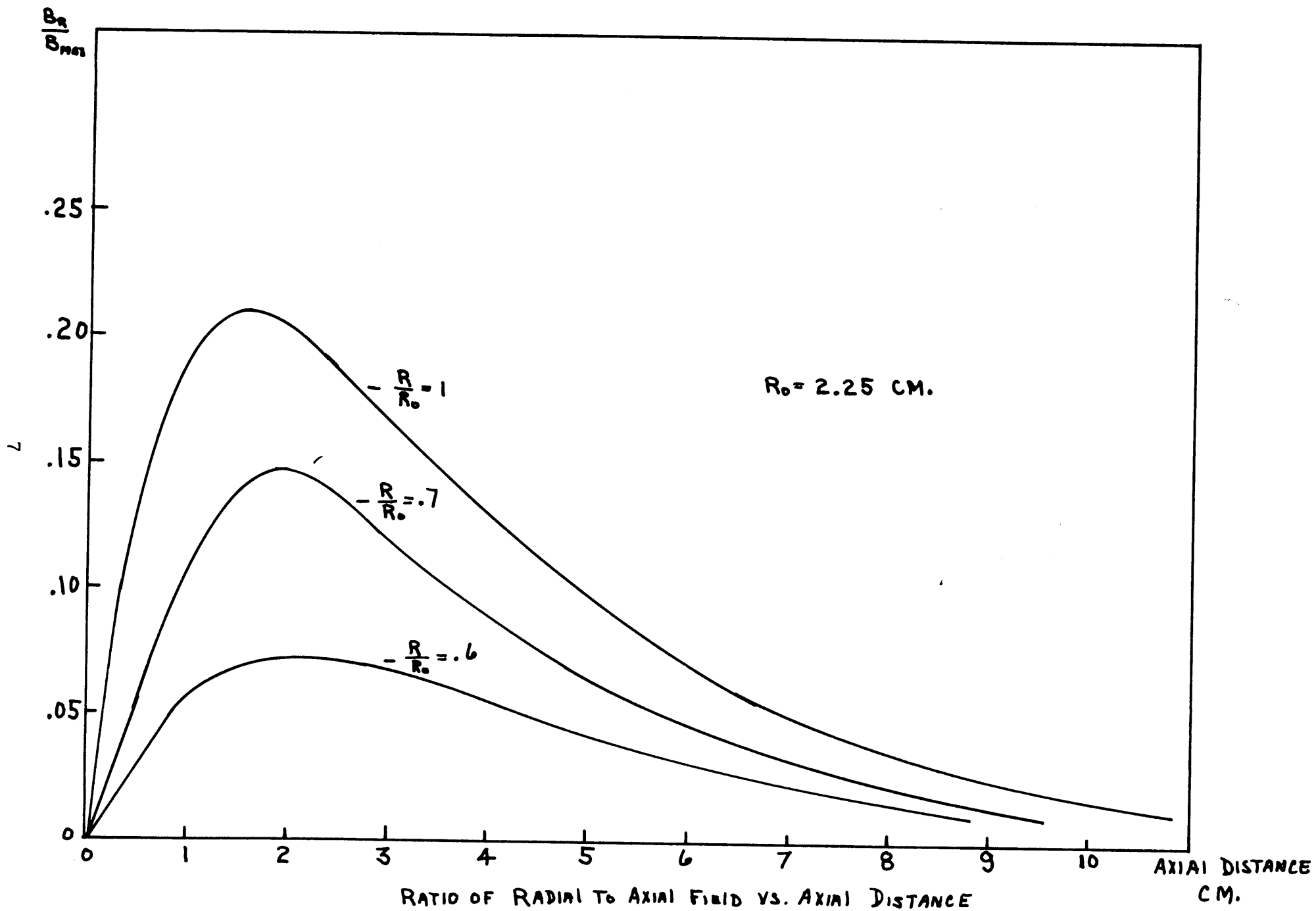RATIO OF RADIAL TO AXIAL FIELD VS. AXIAL DISTANCE

FIG. 3

the radial magnetic field component constant. This curve is plotted along with the experimental curve in Fig. 4.

Effects of Channelling on Reflected Shock

Some qualitative corrections can be made on the theoretical curve of Fig. 4 by considering the effects of channelling on the gas. First, as the plasma is channelled, the increase in density results in the need of a larger force to reflect the shock. This causes the curve of Fig. 4 to shift to the left as shown. Secondly, the area change in the gas, due to channelling, results in the gas seeing lower radial fields as it moves into the coil. The increased density causes a temperature increase as given by the relation

$$\frac{T}{T_o} = \left(\frac{\rho}{\rho_o}\right)^{\gamma-1} \tag{3}$$

which is for a perfect gas under isentropic conditions, where γ is the ratio of specific heats. This combined increase in termperature and density causes the conductivity to increase as shown from the relation by Spitzer[5]
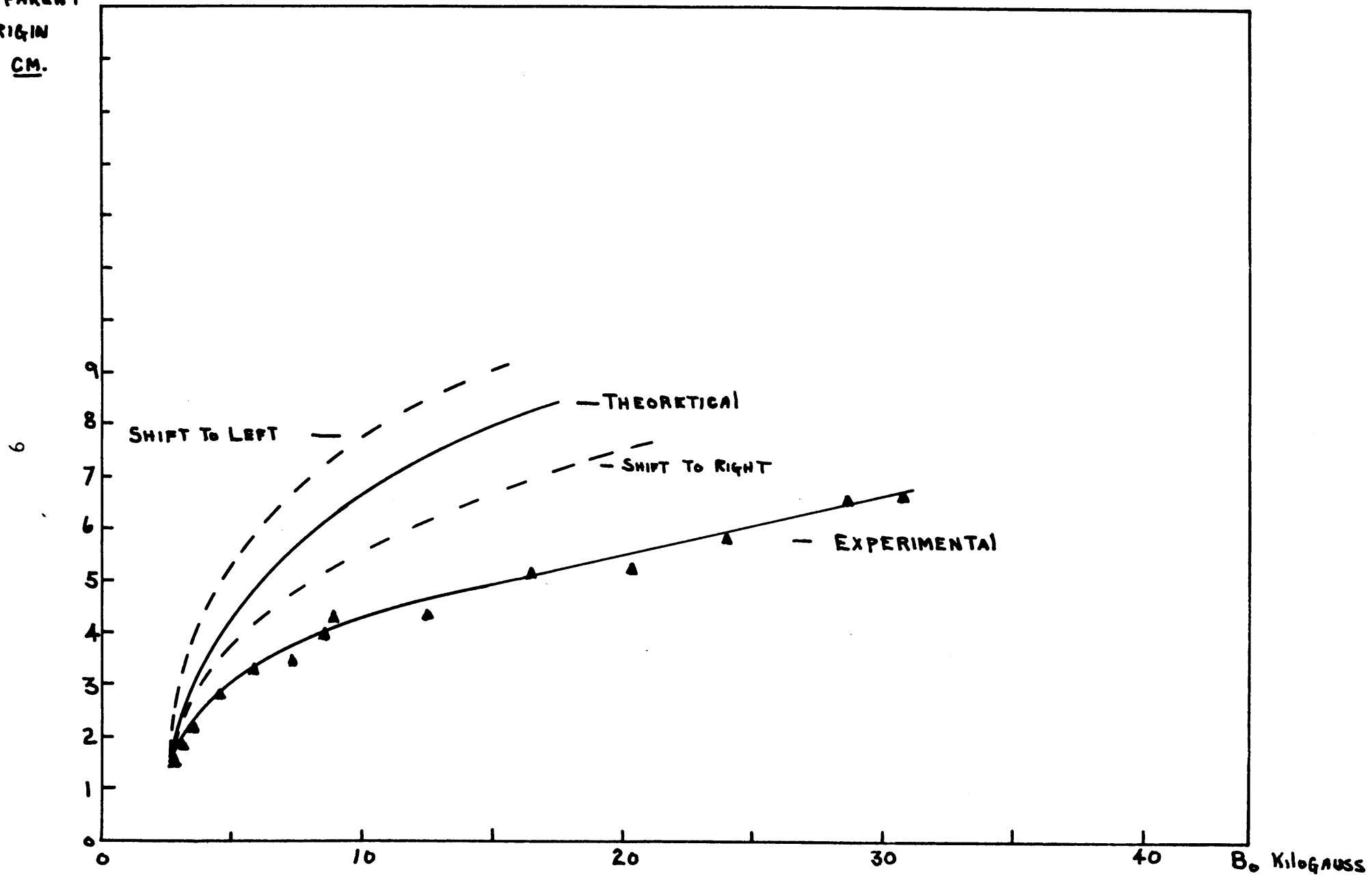
$$\sigma = \frac{1.53 \times 10^{-4} \ T^{3/2}}{\ln \Lambda} \tag{4}$$

where

$$\Lambda = \frac{3}{2e^3} \left(\frac{k^3 T^3}{\pi \eta_e}\right)^{1/2} \tag{5}$$

where σ is the electrical conductivity, k is Boltzmann's constant,

REFLECTED SHOCK ORIGIN VS. AXIAL FIELD STRENGTH B₀

FIG. 4

e is the electronic charge and η_e is the free electron density. This increase in conductivity shifts the curve to the right, since the lower conductivity at far distances from the coil requires an increase in radial field in order to keep the force constant. Finally, the field configuration changes, as shown by the magnetic Reynold's number

$$R_M = \mu \sigma V \ell_c \approx \frac{B_{induced}}{B_{imposed}} \approx \frac{\tau_d}{\tau_t} \tag{6}$$

where μ is the magnetic permeability, ℓ_c is a characteristic length of the interaction (in this case the tube radius), τ_d is the time for the gas to diffuse into the field, and τ_t is the time needed for the gas to travel a characteristic length through the field. These qualitative results are summarized below

Density increase — curve shifts to left

Area decrease — curve shifts to left

σ increase — curve shifts to right

Finally it is desirable to determine a relation between the Mach number of the various shock waves and the magnetic field of the coil. To find an order of magnitude relation, the interaction can be approximated by considering the interaction of a moving shock, impinging on a transverse magnetic field discontinuity as shown in Fig. 5. Both reflected and transmitted shocks are shown. From the modified Navier-Stokes equation

$$\rho \frac{\partial \underline{V}}{\partial t} + \rho (\underline{V} \cdot \nabla) \underline{V} = -\nabla P + \underline{J} \times \underline{B} \tag{7}$$

10

CONTACT DISCONTINUITY

② S_2 T_2 V_2 P_2

④ S_4 T_4 V_4 $P_4^* = P_4 + \dfrac{B_4^2}{2\mu_0}$

M_c

M_b

① P_1 T_1 V_1 S_1

③

⑤ M_a P_0 S_0 T_0 $V_0 = 0$

$P_0^* = P_0 + \dfrac{B_0^2}{2\mu_0}$ S_0 T_0 $V_0 = 0$

t

x
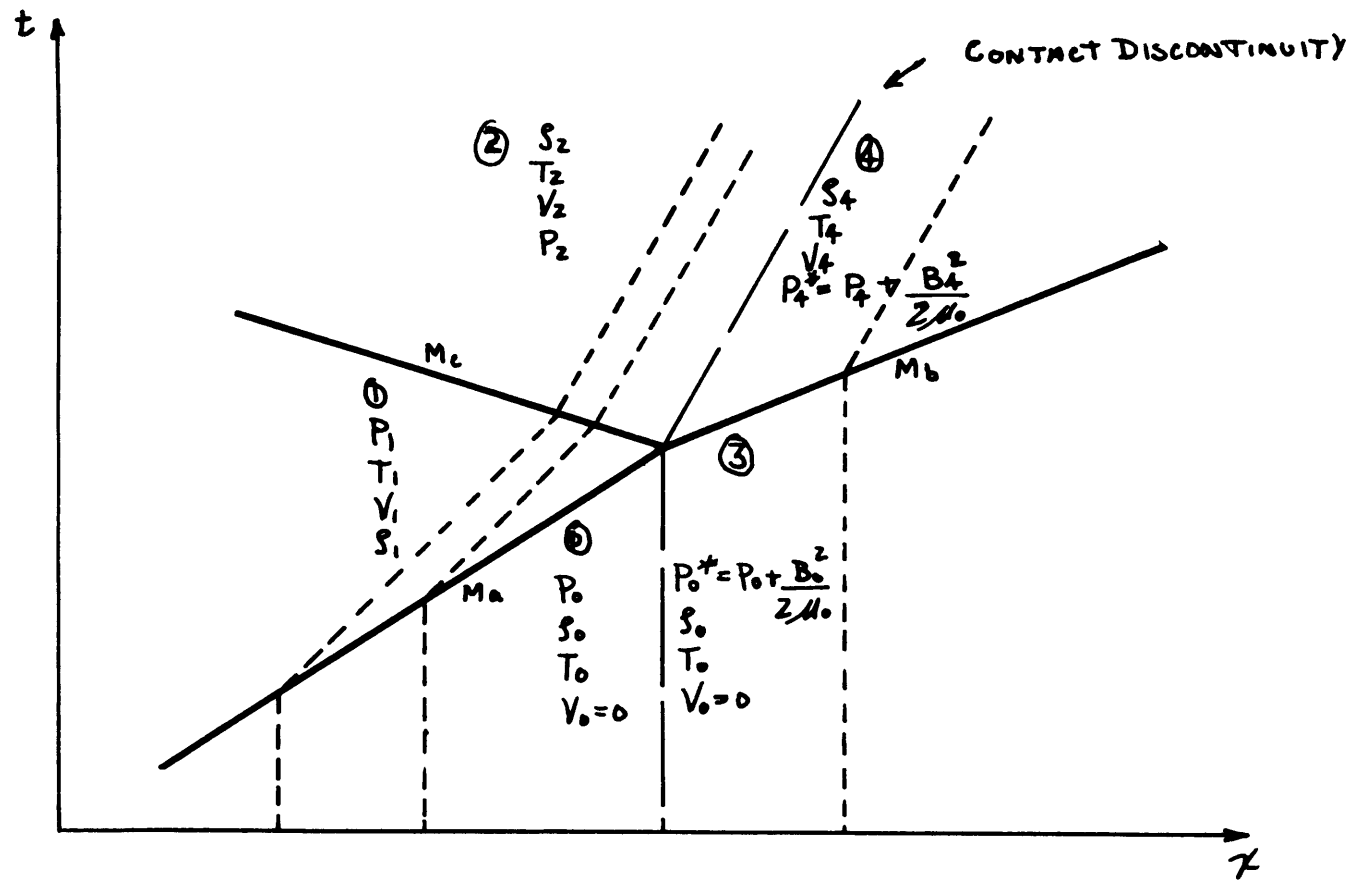
X-t SHOCK DIAGRAM

FIG. 5

it follows, assuming steady flow, that

$$\rho(\underline{V} \cdot \nabla)\underline{V} = - \nabla\left(P + \frac{B^2}{2\mu}\right) + \frac{(\underline{B} \cdot \nabla)\ \underline{B}}{\mu}$$
(8)

This indicates an effective pressure

$$P^* = P + \frac{B^2}{2\mu}$$
(9)

Neglecting ionization effects and channelling, and assuming isentropic steady flow of a perfect inviscid gas, and uniform gas parameters behind the shock, the relation between the pressures across a shock as given by Shapiro[6] is

$$\frac{P_x}{P_y} = \frac{1 + \gamma M_y^2}{1 + \gamma M_x^2}$$
(10)

where x and y refer to parameters of the gas upstream and downstream from the shock front, and M is the Mach number measured from the shock front, based on the local sound velocity. As the plasma impinges on the magnetic wall it slows down, causing a piling up of the gas particles and in the limit, a reflected shock.

In Appendix C, a criterion is developed for which Eq. 10 can be applied to a shock front in a magnetic field using the pressure as defined in Eq. 9. Applying this equation to Fig. 5, results in a fourth degree polynomial in the reflected shock Mach number as a function of the magnetic to static pressure ratio, $\frac{B_o^2}{2\mu_o P_o}$. Under further assumptions this equation is reduced to a quadratic and can be solved for M_c.

Unfortunately only one of the experimental points falls in the region in which we can apply this simplified equation. The theoretical analysis predicts two reflected shock Mach numbers. One of these values violates the assumption used to reduce the equation to a quadratic. The other value predicted is 8.5. The measured Mach number is 3.2. This result is quite satisfactory considering the assumptions necessary to reduce the real problem to the simplified model analyzed. Under these circumstances only an order of magnitude agreement can be expected.

THE EXPERIMENT

Shock Driver

The device used to drive the shock is a set of coaxial electrodes as shown in Fig. 1. The center electrode is hollow in order to make the tube accessible to the vacuum and cold air trap systems. When the driving capacitor is discharged across the electrodes, an aximuthal magnetic field is induced and interacts with the radial currents to create a force on the gas which drives it down the tube. The ohmic dissipation heats the gas to a point where it ionizes. It is heated further through compression by the driving force. Initially the shock front is donut-shaped due to the driver geometry. Therefore all measurements are made four tube diameters away from the driver exit to ensure that the shock front is predominantly planar. Smear camera measurements indicate that this is in fact the case. A disadvantage of this new position is the lower velocity of the plasma when it gets to the coil, due to

13

the kinetic energy lost as it propagates along the tube.

Smear Camera Measurements along Tube

Smear camera measurements made with a slit along the tube are taken with a writing speed of .42 µs/mm. All measurements are made with an initial driver voltage of 24 kv, and initial pressures ranging from .1 mm Hg to 1.0 mm Hg. Fig. 6a is a typical smear camera picture taken along the tube with no applied magnetic field. The thin vertical stripes are centimeter marks made on the shock tube in order to measure distances, while the wide vertical stripe is the field coil. A shock wave is moving to the left, with a reflected shock coming off the end wall of the tube. Fig. 6b is a picture taken with an applied magnetic field of 24,000 gauss. A shock is seen reflecting off the field coil. At this high field a large fraction of the gas does not pass through as verified by the difference in light intensities of the shocks reflecting from the end wall.

A velocity at the field coil versus pressure curve is shown in Fig. 7. Although maximum velocities occur at pressures below .1 mm Hg, all measurements are made at higher pressures because of the higher light intensities produced.

In Fig. 4 an experimental curve is plotted showing the apparent origin of the reflected shock measured with respect to the center of the field coil, versus the axial field value at the coil center. Each apparent origin point is an average of six smear camera measurements. This is necessary due to the difficulty in accurately extrapolating the
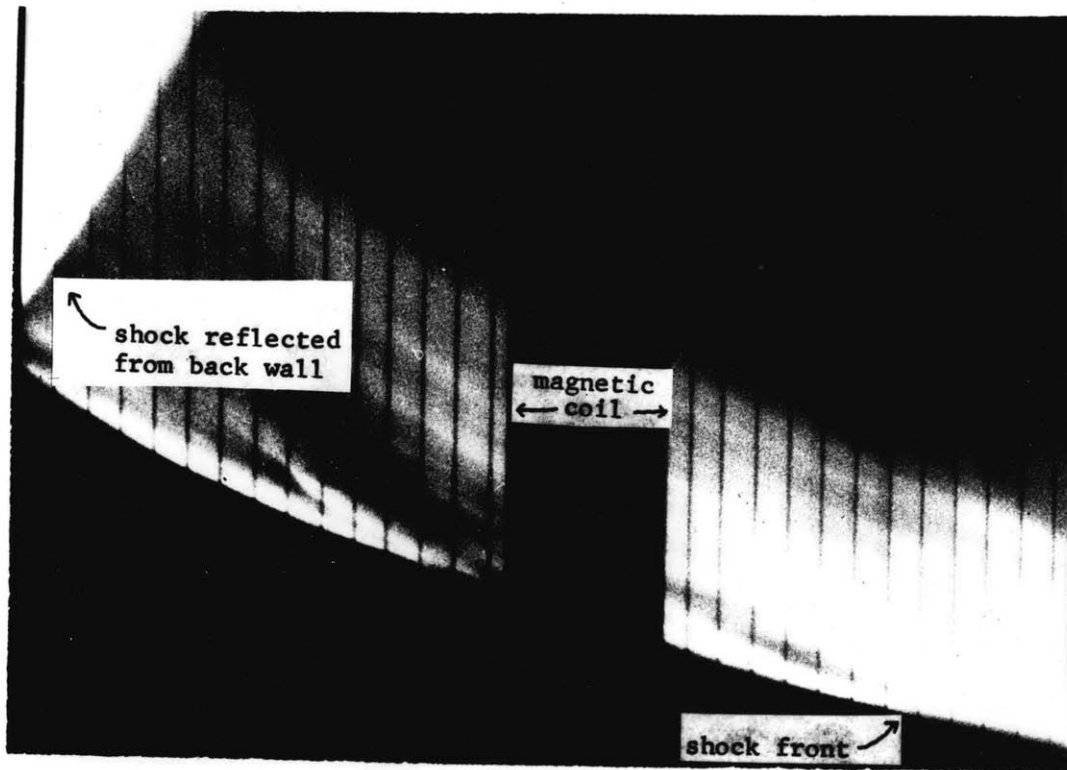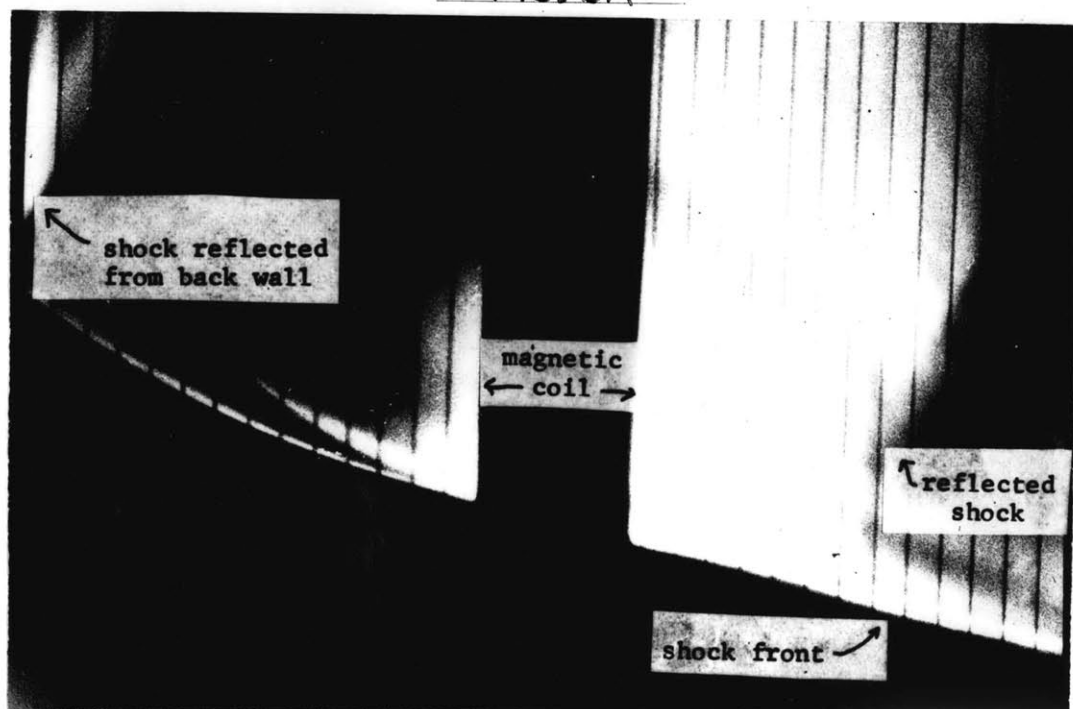
FIG. 6A
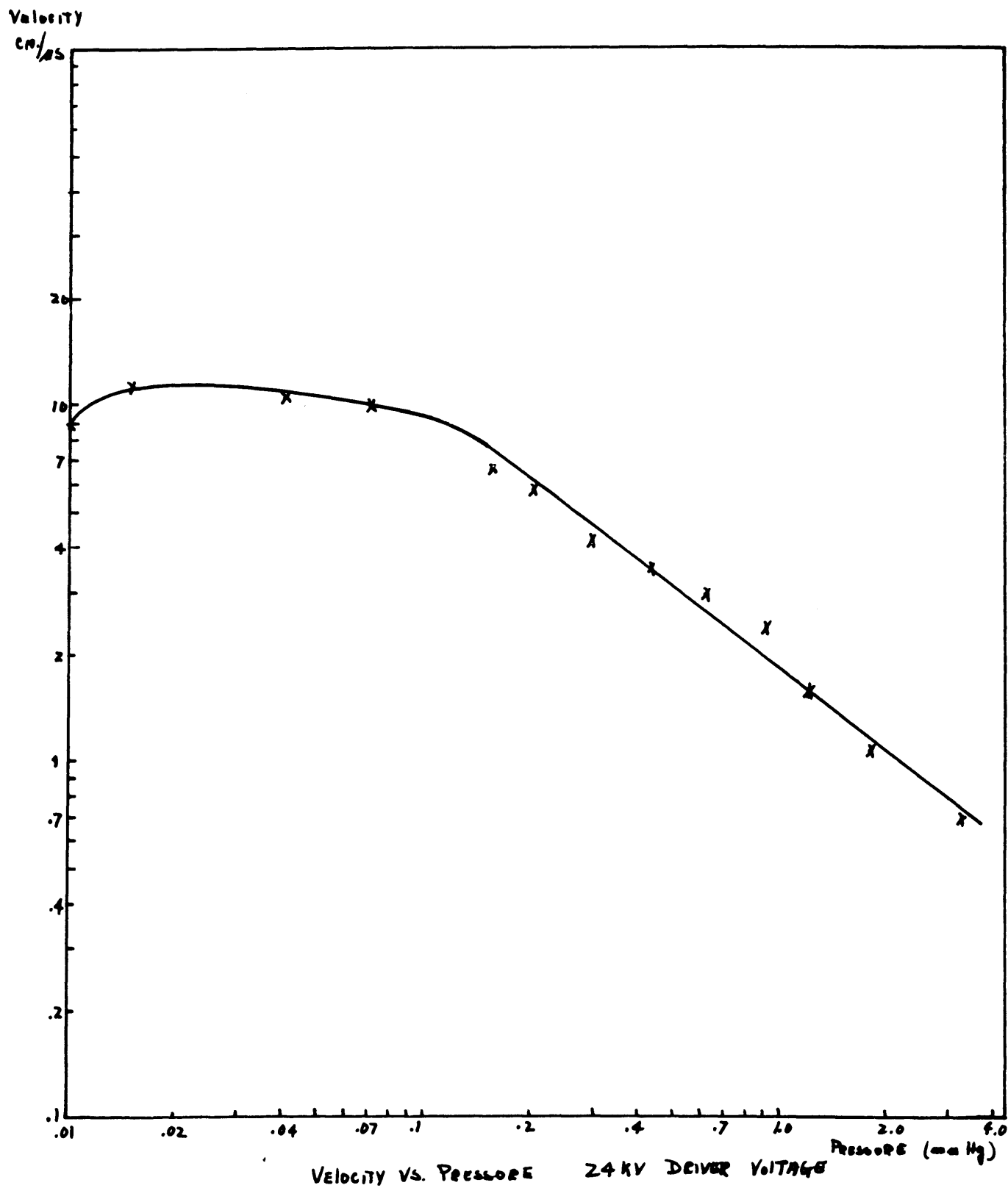

FIG. 6 B

SMEAR CAMERA PICTURES

15

VELOCITY VS. PRESSURE   24 KV DRIVER VOLTAGE

FIG. 7

16

reflected shock front to the origin. The curve verifies,within experimental error, the prediction that the initial shock origin is not less than the peak radial field position of the coil. Also, the curve indicates that the conductivity increases as the gas is channelled in the light of predicted curve discussions. There is also an indication that the reflected shock is formed by the radial field component, since the shapes of the predicted and reflected shock curves are very similar.

Extensive measurements made indicate that there is a threshold field below which a reflected shock does not appear. These data are presented below. Magnetic field values are accurate to ± 30 gauss. The radial field value given is the space average of the radial variation of the applied field at the axial position of the reflected shock.

Initial Pressure (mm Hg)	B_r Average (gauss)	Initial Apparent Origin (cm)	Reflected shock Velocity (cm/μs)
.1	–	no reflected shock observed	–
.2	–	no reflected shock observed	–
.3	300	1.3	.47
.4	220	1.4	.43
.5	165	1.5	.54
.6	165	2.1	.60
.7	165	2.0	.65
.8	165	2.5	.55
.9	140	3.0	.63

The value of the static B_r is not necessarily the field actually

reflecting the shock because the gas changes the field configuration. Below .2 mm Hg no reflected shocks can be observed for applied fields up to 30,000 gauss. The low ratio of Larmor frequency to collision frequency indicates that this is not due to the particles following the magnetic field lines at these low pressures. It is possible that a reflected shock is present, but the light output is too low to be seen due to the gas densities.

Flux Excluded Curves

A ten turn pickup coil in a shielded copper enclosure is placed on the tube so that it measures axial flux. The output of this coil is put into a .1 sec time constant integrator and is observed on an oscilliscope. By measuring the integral of the induced voltage and taking its ratio to the applied flux, a plot can be constructed of this ratio versus applied magnetic field.

The curve presented in Fig. 8, indicates that the gas is being channelled as the field is increased because the flux-excluded ratio is dropping. However, definite information concerning the cross sectional area change of the shock cannot be obtained from this plot alone, because a change in conductivity also affects the shape of the curve.

Smear Camera Pictures of Slit Across Tube

By placing a slit across the tube one centimeter upstream from the field coil, a smear camera photograph of the shock can be taken as it enters the magnetic field. Pictures are taken at 650 cps (.32 μs/mm

18

.3 MM. Hq. 20KV

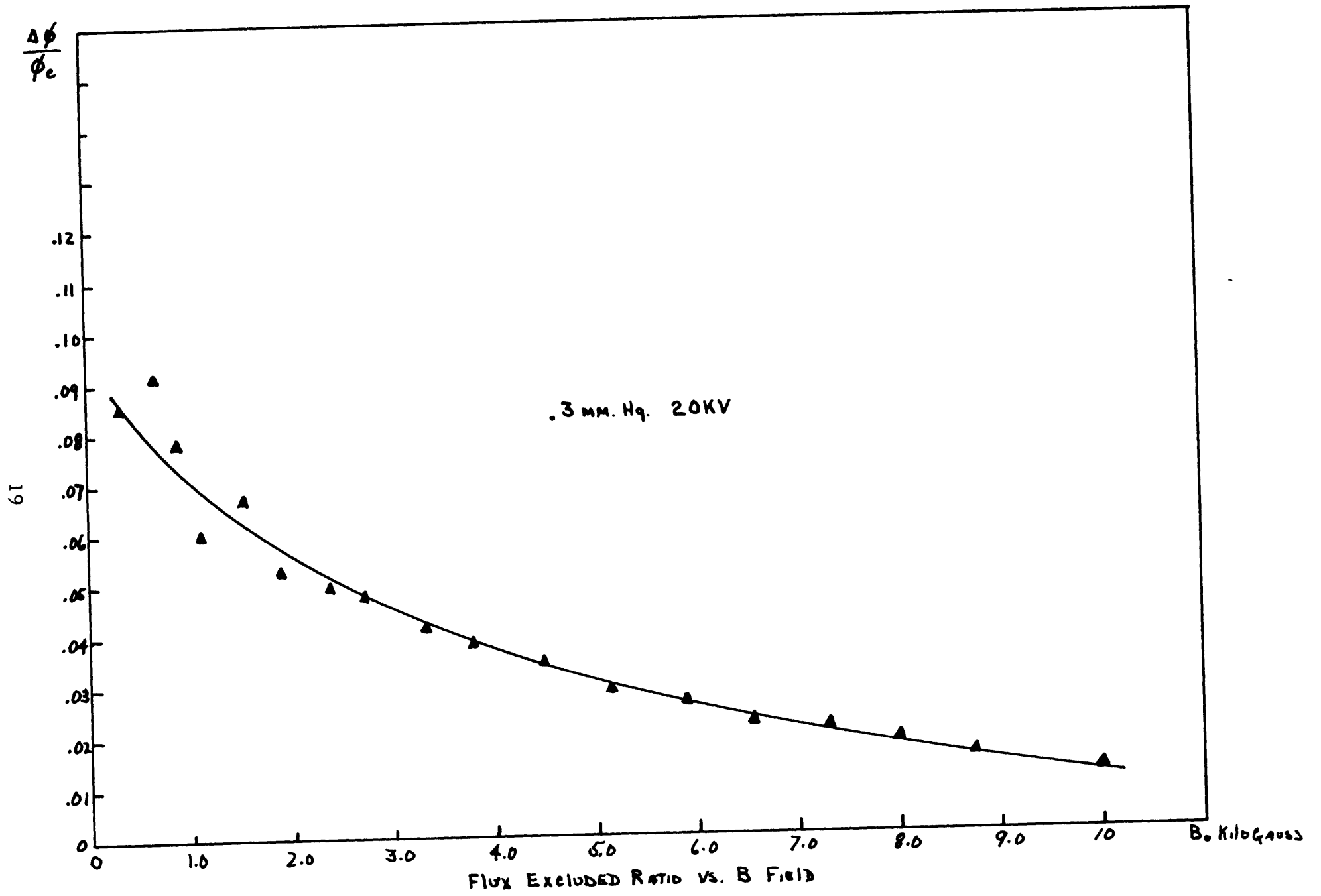Flux Excluded Ratio vs. B Field

Fig. 8

writing speed), for various applied magnetic fields. Fig. 9 shows

three pictures taken across the tube with the shocks moving to the

left. Fig. 9a is with no applied field. The shock front is planar, but

the gas behind is turbulent and not uniform. Figs. 9b and 9c are with

applied fields of 8,000 and 20,000 gauss respectively. The plasma

is strongly channelled as demonstrated by these photographs. The

incoming velocities of all these pictures are about the same. However,

the gas diffuses back into the magnetic field in much less time in

Fig. 9b, then in Fig. 9c. This diffusion time increase indicates that

the magnetic Reynold's number and therefore the conductivity of the

gas have increased considerably, in view of Eq. 6.

RESULTS AND CONCLUSIONS

The experimental data taken indicate two important results con-

cerning the interaction of a plasma with the magnetic field of a sole-

noidal coil.

First, a reflected shock wave is produced purly through the inter-

action of the radial field component and the plasma. This shock is

formed further upstream from the field coil as the magnetic field is

increased. Also, as the gas enters the coil it is channelled as the

magnetic field intensifies, so that the field coil looks like a nozzle to

the gas.

Finally the conductivity increases considerably as the gas is com-

pressed. This indicates that a design for an energy converter need

not require magnetic Reynold's numbers as high as calculated, because

9A

9B

9C
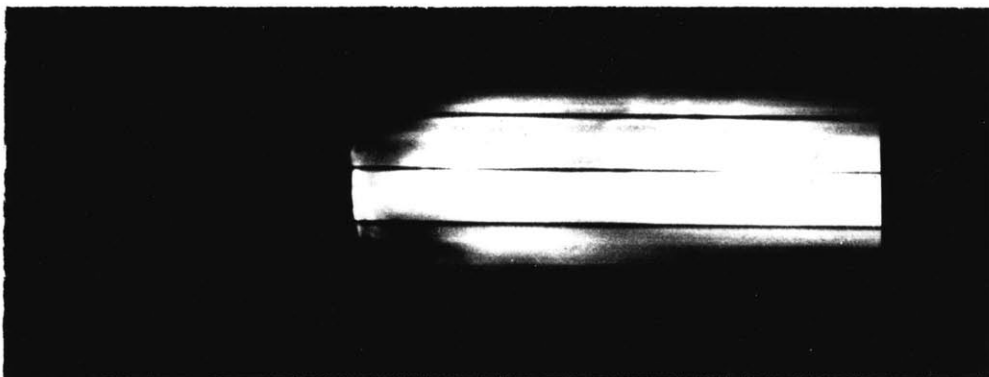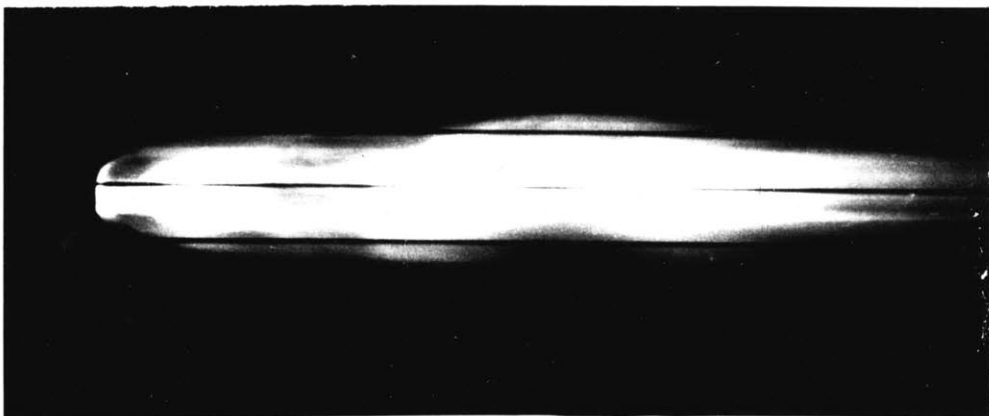
FIG 9

the conductivity and magnetic Reynold's number increase as the plasma enters the field coil.

These results indicate a need to investigate the amount that the magnetic Reynold's number grows through this effect. As the magnetic field is increased further the magnetic Reynold's number will drop since the nozzle effects of the coil begin to choke off the plasma and decrease the velocity. An experimental investigation of this effect should be made to find the optimum amount of channelling to acquire a maximum value of R_M.

Finally, measurements should be made with a smear camera across the tube to find the area ratio of the plasma as the magnetic field is intensified. Using these data, information can be extrapolated from the flux-excluded-ratio curves, to obtain information about the conductivity of the gas as the magnetic field of the coil is increased.

APPENDIX A

MAGNETIC PULSE CIRCUITS

Introduction

A large-current pulse circuit is used to produce magnetic fields whose duration is long compared to the travel time of a shock wave. Two systems are used to give variable magnetic fields over the full range from 900-30,000 gauss.

Small Pulse System

The fundamental circuit used is a thyratron in series with a charged capacitor and the field coil. This circuit produces a half cycle of a sinusoidal time-varying field. Fig. A-1.1 shows the complete circuit. With the second thyratron removed, the waveforms are as shown in Fig. A-1.2. There are two disadvantages to this circuit as it stands. For high initial voltages, the reversal ratings on most oil capacitors are exceeded. Secondly the duration of the maximum field is relatively short compared to the total pulse length. Both problems are solved by placing thyratron (2) in the circuit biased "on" as shown. The system is initiated by pulsing the grid of thyratron (1). During the first quarter cycle thyratron (2) is back biased from plate to cathode by the voltage across the field coil. When this voltage passes through zero, the second thyratron conducts the current to produce an RL decay. The waveforms appear in Fig. A-1.3.

Parameters of Small System:

Field coil: Solenoidal coil - 2.5 cm inside radius, 6 cm outside

30 KV POWER SUPPLY

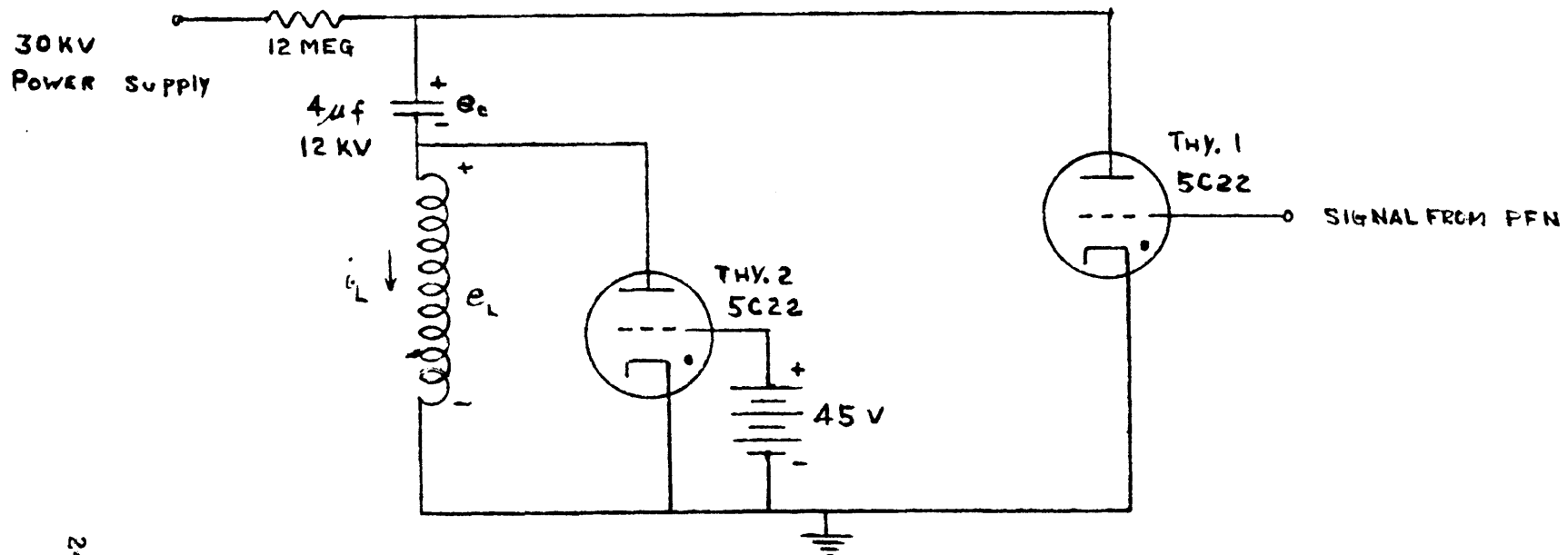12 MEG

$4\mu f$ 12 KV

e_c

i_L

e_L

THY. 2 5C22

45 V

THY. 1 5C22

SIGNAL FROM PFN

Fig. A-1.1

$-e_c$

e_L

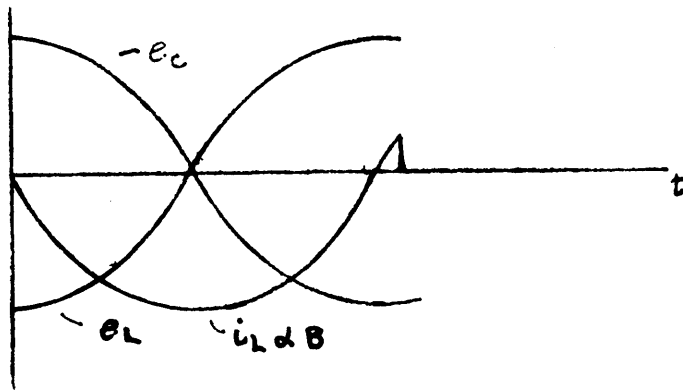$i_L \propto B$

t

Fig. A-1.2

$-e_c$

e_L

$i_L \propto B$

t
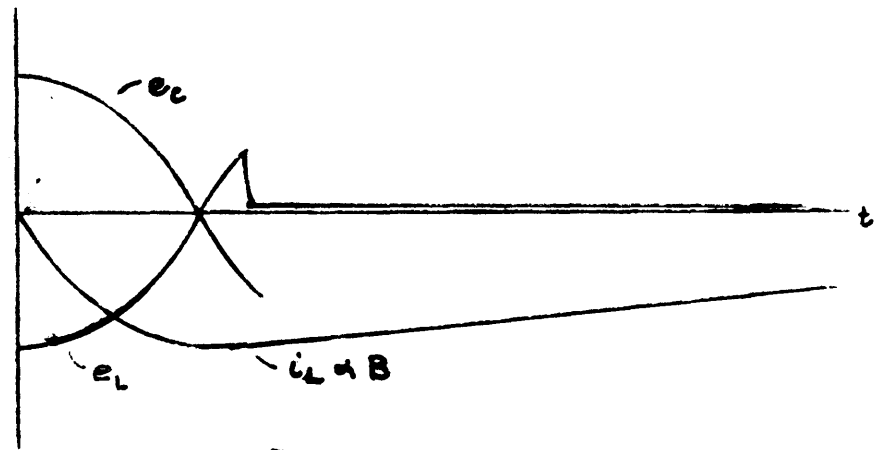
Fig. A-1.3

THYRATRON PULSE CIRCUIT & WAVEFORMS

Fig. A-1

24

radius - 3.5 cm thick; 720 turns No. 14 formvar copper wire; induct-
ance $\approx$ 24 mh.

Capacitor: 4 μf - 12 kv max.

Thyratron: 5C22 hydrogen - 16 kv, 350 amps peak.

Ringing frequency: ~ 500 cps.

Field range: 500-9,000 gauss.

Large Pulse System

The large system is similar to the circuit of Fig. A-1.1 with the
circuit elements changed. The network is shown in Fig. A-2. The
thyratrons used in the small system are replaced by ignitrons which
have a current carrying capacity of 35,000 amps. The circuit used
to fire these ignitrons is essentially the thyratron circuit described
above with different element values. The ringing frequency of the
thyratron circuit is slightly higher than the ringing frequency of the
ignitron circuit so that I_2 is ignited before the voltage on the field coil
forward biases the ignitron. When the current through the field coil
goes through the peak of the sine wave, ignitron (2) is switched on and
conducts, producing waveforms much like those of Fig. A-1.3. The
capacitor in the trigger circuit is charged to 2.1 kv. The 400 μf
capacitor is charged from 200 to 4,000 volts, depending on the mag-
netic field desired.

A. Trigger Circuit

Thyratron: 5C22 hydrogen - 16 kv peak voltage - 350 amps peak
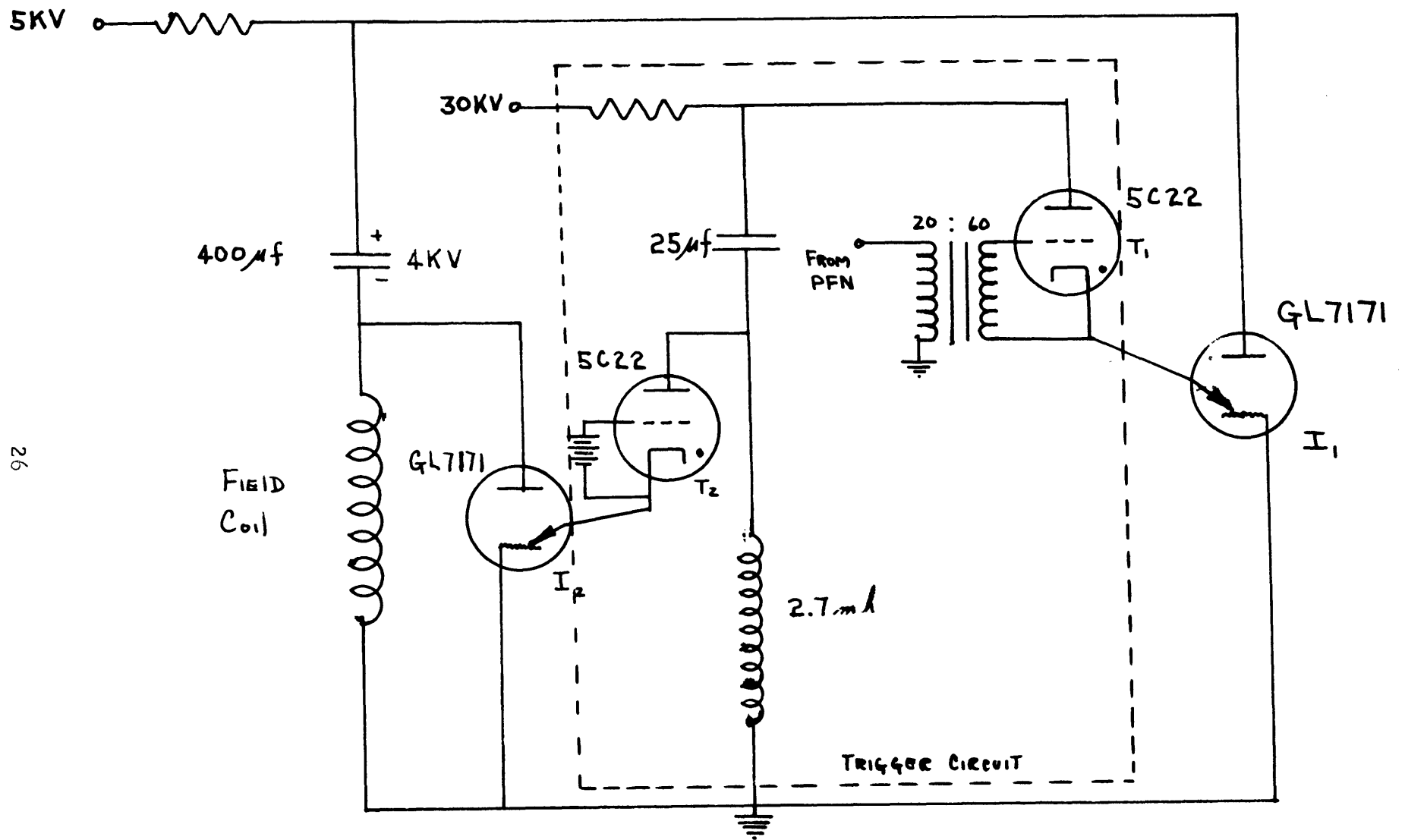
Ignitron Pulse Circuit

Fig. A-2

Capacitor: 25 µf – 4 kv.

Coil: 2.7 mh coil.

Ringing frequency: ≈ 640 cps.

B. Ignitron Circuit

Ignitron: GL7171 General Electric

10 kv – 35 ka peak – air cooled.

Capacitor: 400 µf – 4 kv.

Field Coil: 300 µh – 64 turns – 4 in hand No. 12 formvar copper wire on solenoidal form ID – 2.5 cm; OD – 6 cm; 3.5 cm thick potted with stycast 4030 compound.

Ringing frequency: 460 cps.

Field Range: 2 – 30 kilogauss.

The system is constructed in a container provided with forced air circulation. An infrared heat lamp is used to maintain the required anode to cathode temperature gradient. Thermocouples are used to measure this gradient. The main conductors to the ignitrons are constructed with copper tubing. The constructed device is shown in a top view, in Fig. A-3.

FIG. A-3

28
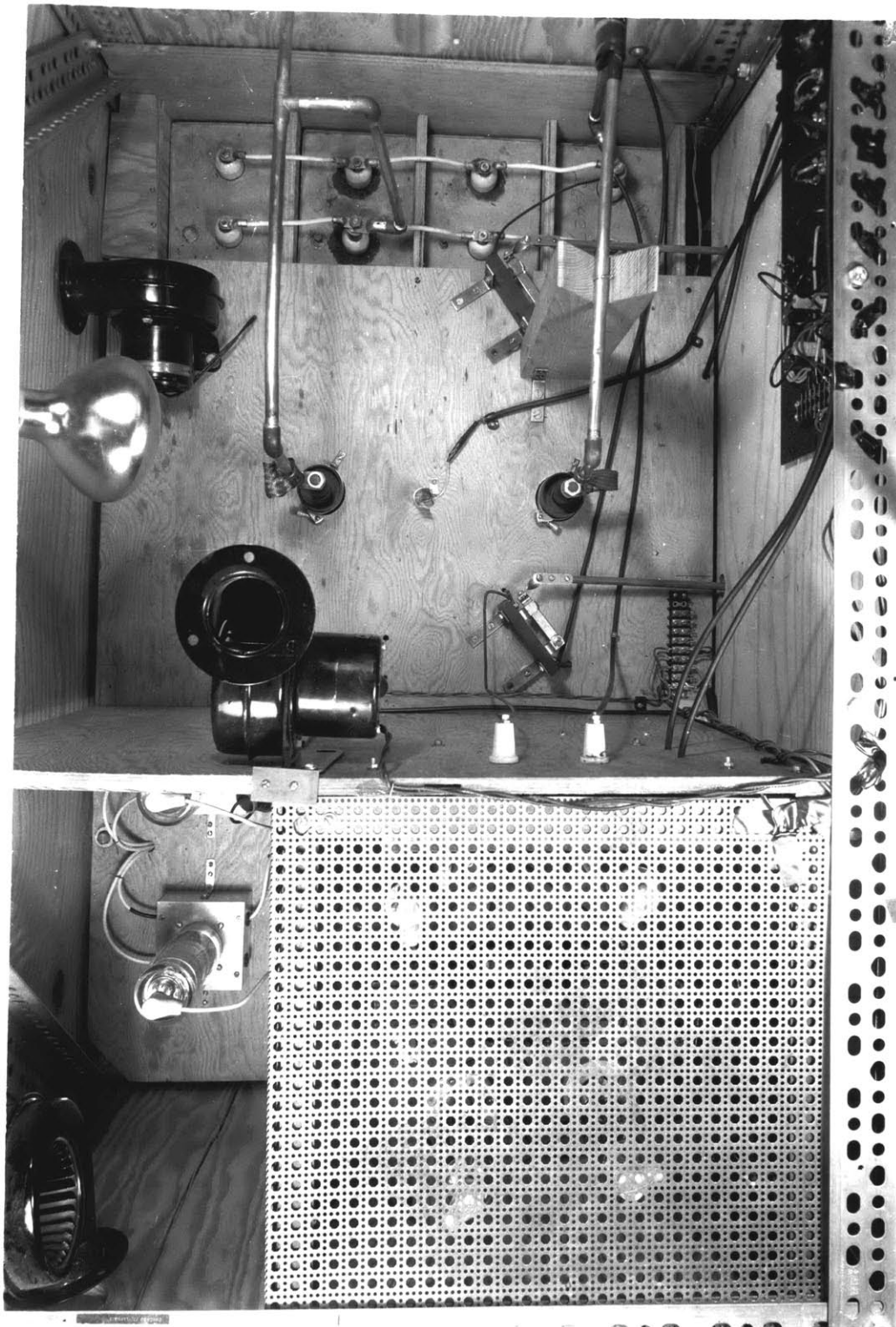
APPENDIX B

SMEAR CAMERA AND TIMING SYSTEM

In order to make repeatable smear camera pictures, an accurate timing system was needed. The design is versatile in that delay times are adjustable and the camera can be operated at different speeds with ease.

The camera is a high speed induction motor running single phase connected through a bellows coupling to a flat mirror. The light from the shock tube is focused on a sheet of film placed on a circle of 40 cm radius from the mirror. The light coming from the shock tube is swept across this sheet of film by the rotating mirror, making a distance versus time history of the shock.

A starting pulse for the system is obtained by reflecting a beam of light off a thin reflecting strip mounted on the bellows, into a 931 A photomultiplier, as shown in Fig. B-1. This pulse is amplified and enters a gate circuit which is the initial stage of the timing system shown in Fig. B-2. The gate circuit consists of a tube initially cut off. Upon switching the tube into the amplification region the pulses are passed to the grid of a 2D21 thyratron which is in series with an LC circuit. When the thyratron is actuated, the initially charged capacitor discharges into the inductor and the usual oscillation begins, and lasts one-half cycle until the thyratron is extinguished by the current reversal. The output voltage seen across the inductor serves as a pulse. This pulse is used to initiate the first delay. This same pulse

29

FILM

SHOCK FRONT

PHOTOMULTIPLIER

REFLECTING STRIP

LIGHT SOURCE

SHOCK TUBE
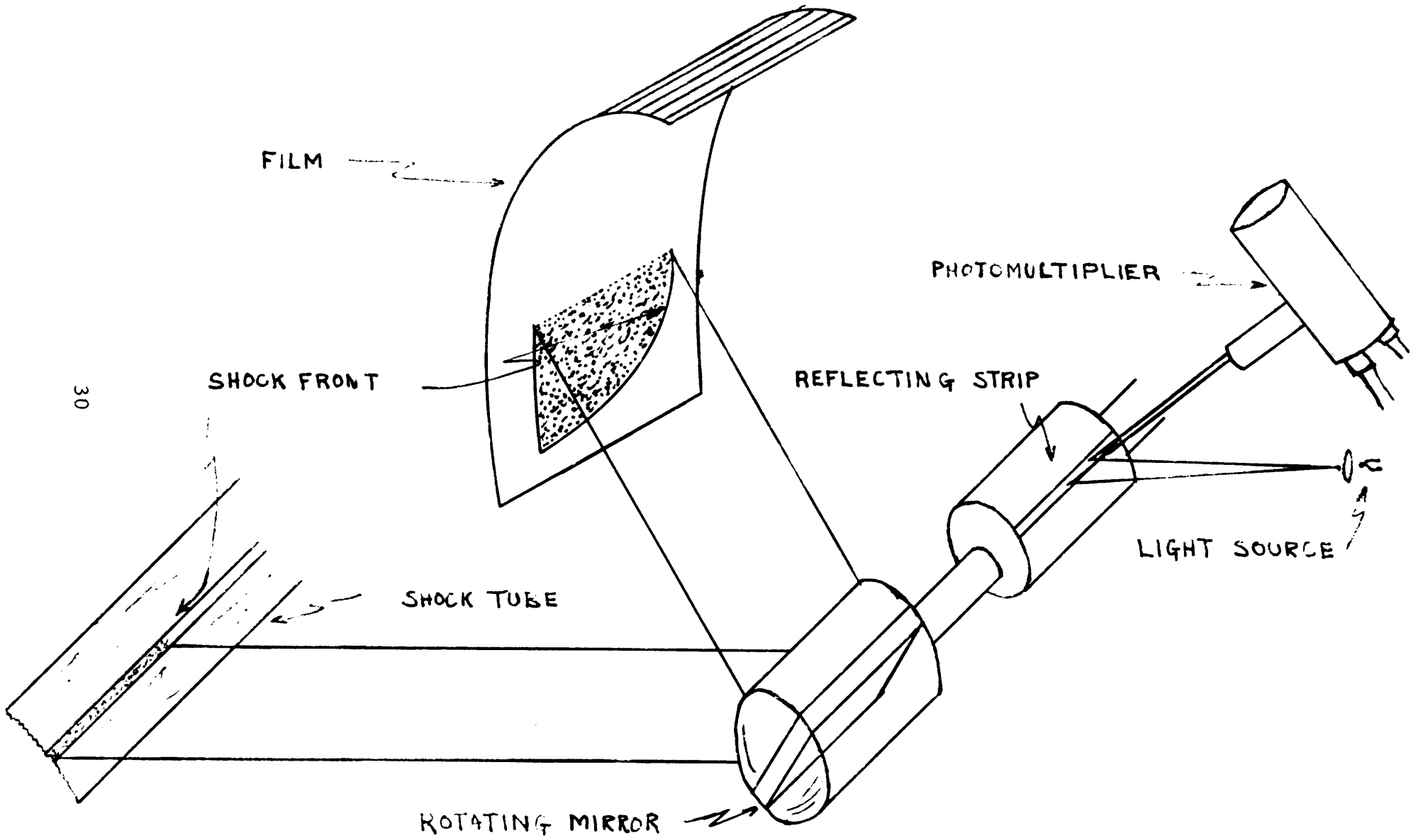
ROTATING MIRROR

Rotating Mirror Camera Geometry

Fig. B-1

31

```
┌───────────────┐        ┌──────────┐      ┌──────────┐      ┌──────────────┐      ┌──────────┐      ┌──────────┐
│ Photomultiplier│───────│   GATE   │──────│  PFN 1   │──────│    DELAY     │──────│  PFN  2  │──────│  DELAY   │
└───────────────┘        │ CIRCUIT  │      └──────────┘      │  CIRCUIT 1   │      └──────────┘      │ CIRCUIT2 │
                         └────┬─────┘                        └──────────────┘         │              └────┬─────┘
                              │                                                  ┌────┴────┐             │
                              │                                                  │  MAG.   │        ┌────┴─────┐
                         ┌────┴─────┐                                            │  FIELD  │        │  P. F. N │
                         │ STARTING │                                            └─────────┘        │     3    │
                         │  SWITCH  │                                                               └────┬─────┘
                         └──────────┘                                                                    │
                                                                                                    ┌────┴─────┐
                                                                                                    │  SHOCK   │
                                                                                                    │ TRIGGER  │
                                                                                                    └──────────┘
```
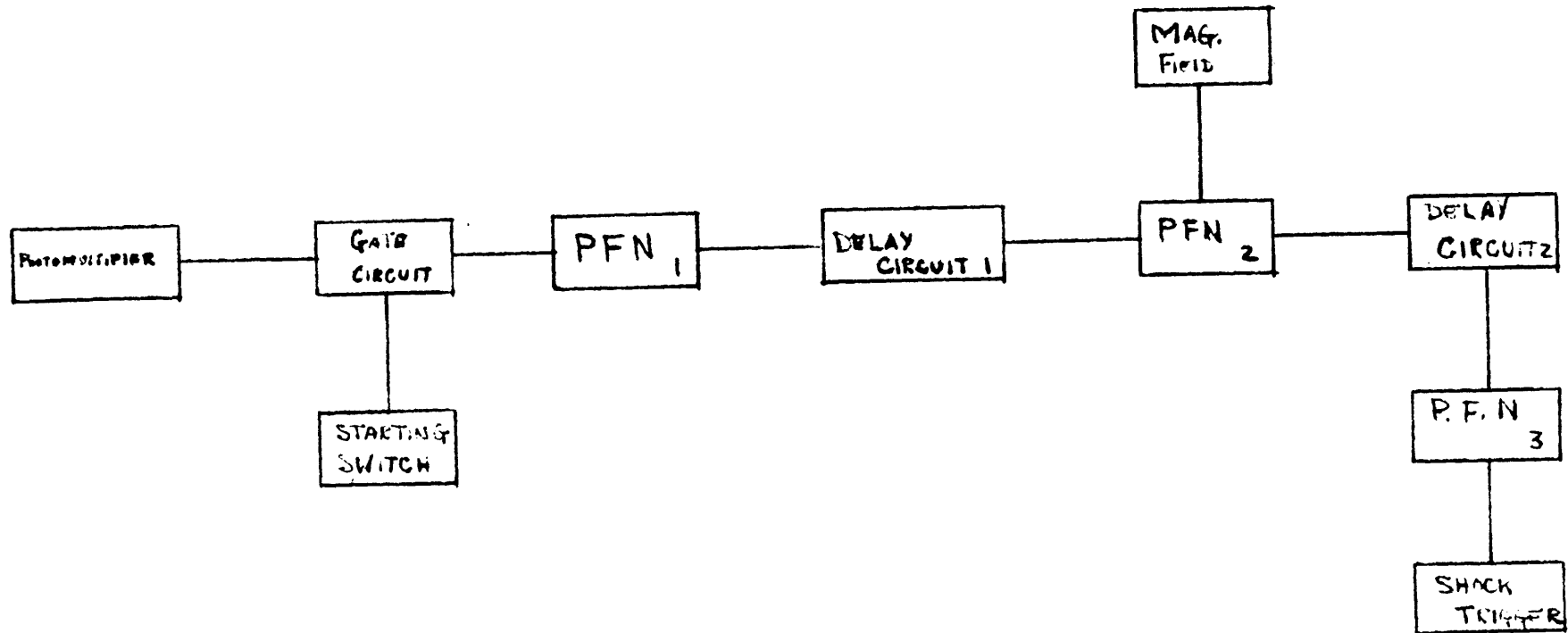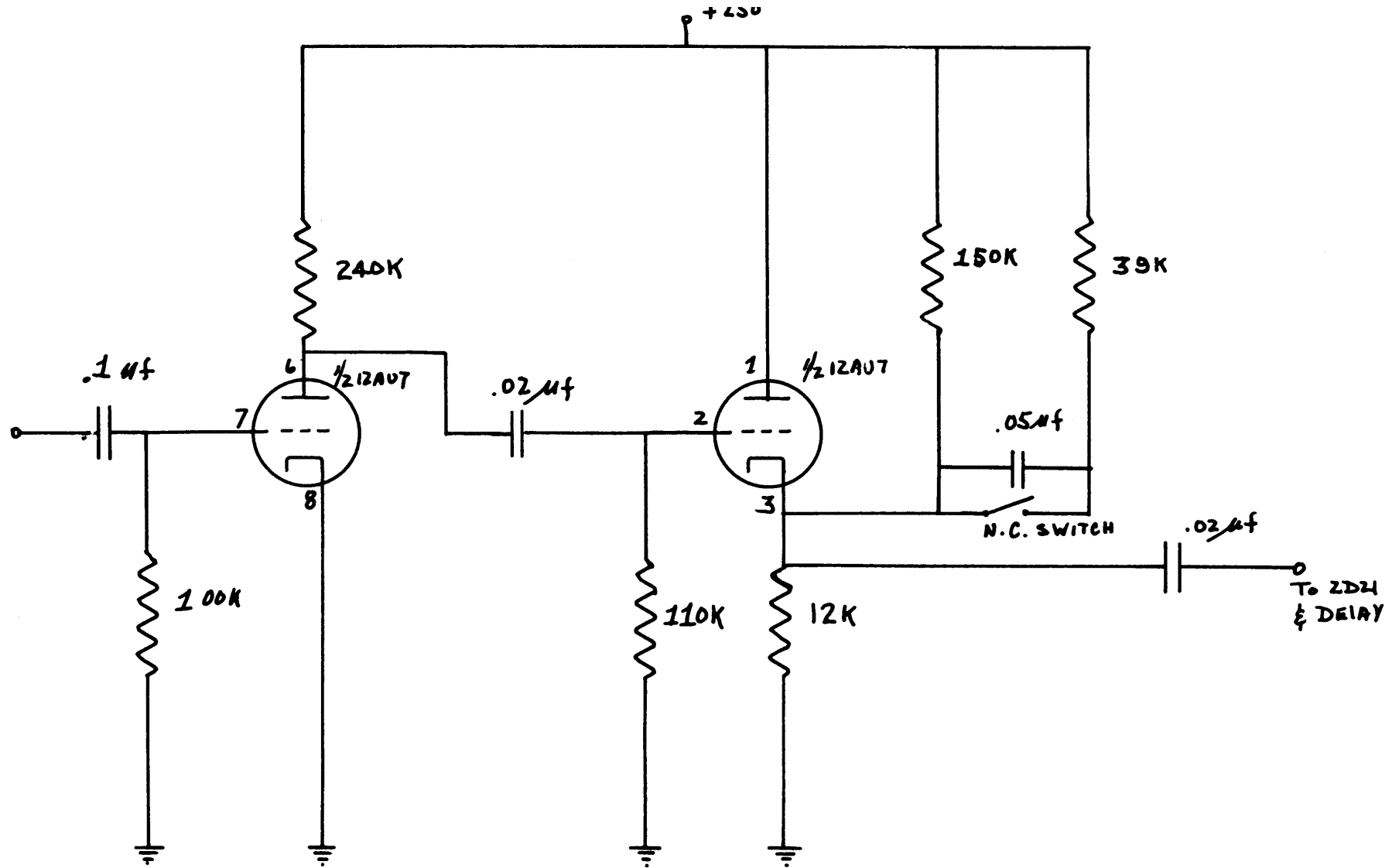
TIMING   SYSTEM

FIG. B- 2

circuit is used as a trigger for the magnetic field supply and delay (2), as well as an initiating signal for the shock tube trigger.

The delay circuit (2) is set to fire the tube when the magnetic field is at a peak value. Delay (1) is set to synchronize the smear camera mirror with the shock tube trigger. The gate, delay and pulse forming networks are shown in Figs. B-3 and B-4. Fig. B-5 shows the smear camera and timing system with associated controls.

Results

When the camera is rotating 30,000 rpm (.42 μs/mm writing speed) the maximum time jitter allowed is 8 μs. The jitter of the total system is less than 1 μs, with 98 per cent of attempted shots successful.

AMPLIFIER & CAMERA GATE CIRCUIT

FIG. B-3

e_{IN}

−

+

100K 2W

.005μF

6

V1

2D21

1,5,7

3 4 2

20K 10W

1M

100K 2W

500K 2W

−400 V.D.C.

THORDARSON T-21FOB

115 VAC 60~

50μH

1μF

2D21 OUTPUT (NOT USED WITH CAMERA CIRCUIT)

1N39

+250V

9.5K 2W

1M POT

50K

.001μF

1M

9.5K 2W

.003μF

.03μF

SW1

100μμF

V3 ½ 12AU7 1

1

2

V2 12AU7

3

30μμF

7

6

8

2

3

1μF

DELAY OUTPUT

1M

3K

100K

1M

12.3K 2W

6.3VAC

5

9 9

4 4

V2 V3

9-14-60 J.E.T.

2D21 TRIGGER & DELAY CIRCUIT
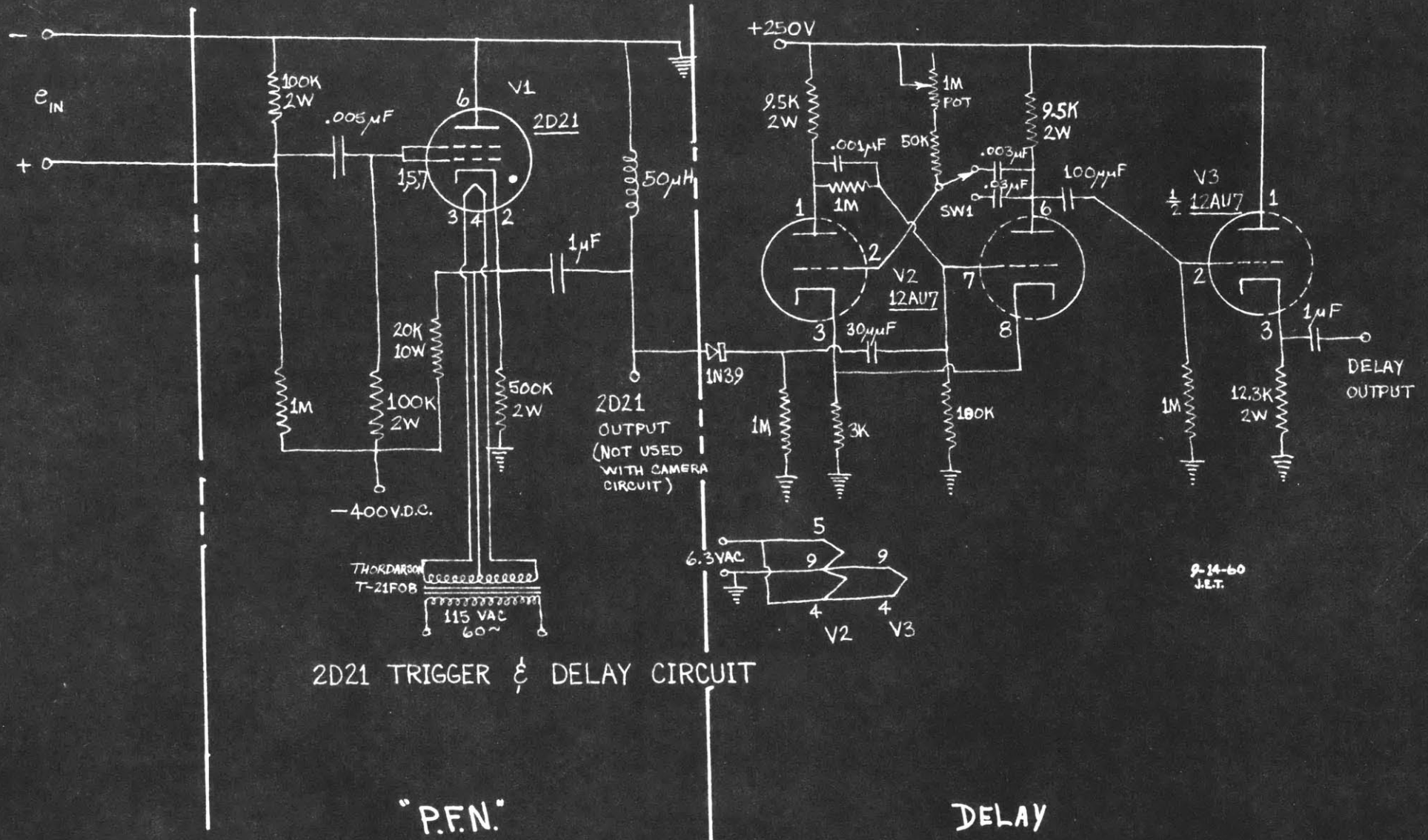
"P.F.N."
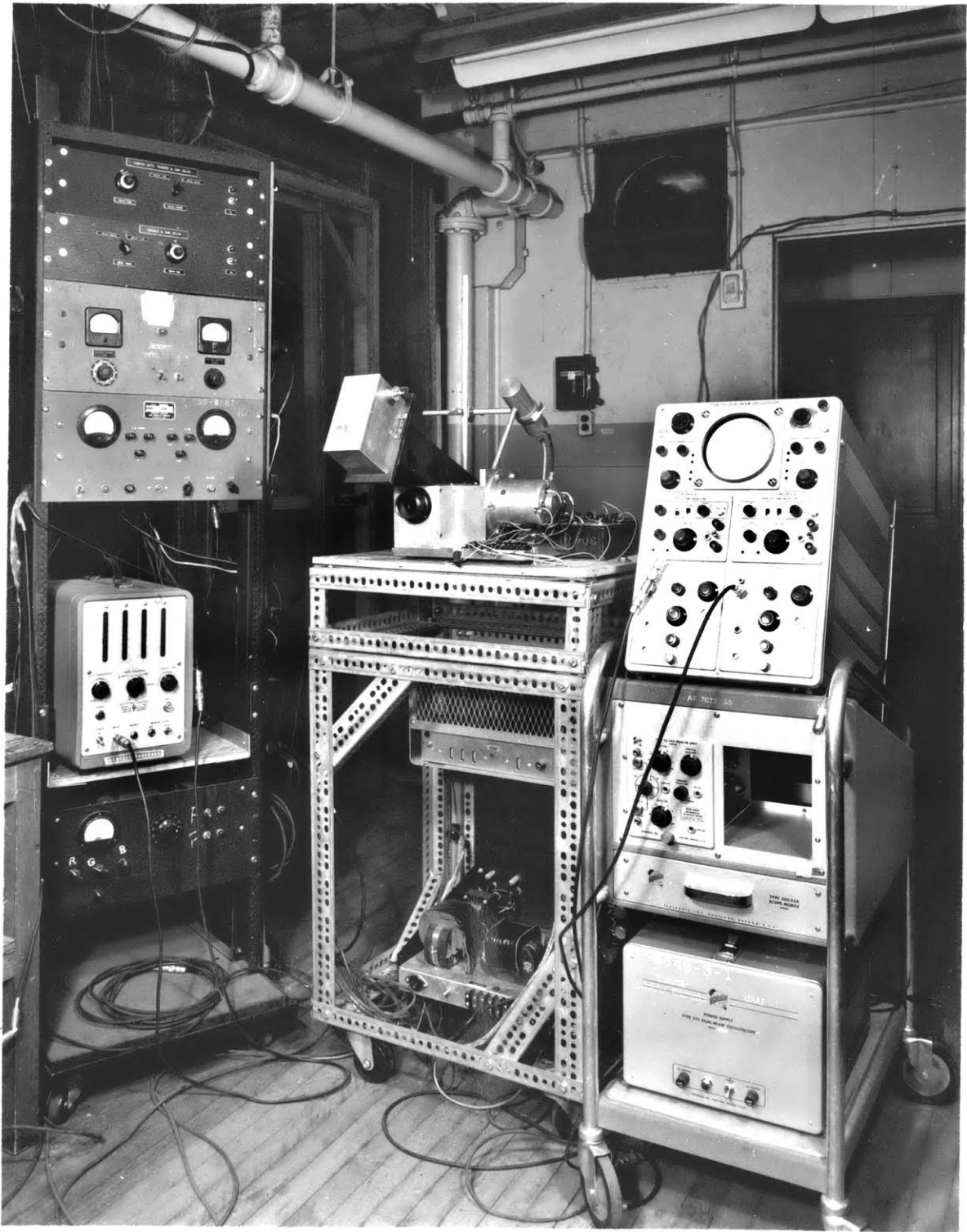
DELAY

FIG. B-4

34

FIG B-5

35

APPENDIX C

In Fig. 5 it is assumed that the pressure in the magnetic field region can be represented by

$$P^* = P + \frac{B^2}{2\mu} \qquad \text{(C-1)}$$

as given in Eq. 9. It is necessary to determine the region in which the ordinary gas dynamic relations can be applied to this new pressure. Assuming steady state, isentropic inviscid flow of a perfect gas, with uniform properties behind the shock and neglecting ionization, the equations governing the motion are,

Continuity: $\rho_o U_o = \rho_1 U_1$ (C-2)

Momentum: $P_o + \rho_o U_o^2 + \frac{B_o^2}{2\mu_o} = P_1 + \rho_1 U_1^2 + \frac{B_1^2}{2\mu_o}$ (C-3)

Energy: $\frac{\gamma}{\gamma-1}\left(\frac{P_o}{\rho_o}\right) + \frac{B_o^2}{\mu_o \rho_o} + \frac{U_o^2}{2} = \frac{\gamma}{\gamma-1}\left(\frac{P_1}{\rho_1}\right) + \frac{B_1^2}{2\mu_o} + \frac{U_1^2}{2}$ (C-4)

For perfect conductivity

$$\frac{B_o}{\rho_o} = \frac{B_1}{\rho_1} \qquad \text{(C-5)}$$

Eliminating ρ_1, U_1, and P_1 in these equations,

$$\frac{P_o}{\rho_o} + U_o^2 + \frac{B_o^2}{2\rho_o\mu_o} - \frac{U_o^2 B_o}{B_1} - \frac{B_1^2}{2\rho_o\mu_o} = \frac{B_1 P_o}{\rho_o B_o} + \frac{B_o B_1 (\gamma-1)}{\rho_o \gamma \mu_o} + \frac{B_1(\gamma-1) U_o^2}{2B\gamma}$$

$$- \frac{B_1^2(\gamma-1)}{\rho_o \mu_o \gamma} - \frac{B_o U_o^2 (\gamma-1)}{2B_1 \gamma} \qquad \text{(C-6)}$$

Let

$$S = \frac{C_a^2}{C_o^2} = \frac{B_o^2}{\gamma P_o \mu_o} \tag{C-7}$$

where

$$C_a = \sqrt{\frac{B_o}{\rho_o \mu_o}} = \text{Alfven velocity} \tag{C-8}$$

and

$$C_o = \sqrt{\frac{\gamma P_o}{\rho_o}} = \text{Sound velocity} \tag{C-9}$$

and

$$M_o = \frac{U_o}{\sqrt{\left(\frac{\gamma P_o}{\rho_o}\right)}} = \text{Mach number} \tag{C-10}$$

Employing these to simplify Eq. C-6:

$$\frac{x - x^2}{\gamma - 1} + \frac{M_o^2}{2}\left(x - \frac{2\gamma x^2}{\gamma - 1} + \frac{\gamma + 1}{\gamma - 1}x^3\right) = S\left(\frac{(\gamma - 2)}{2(\gamma - 1)} - x + \frac{\gamma}{2(\gamma - 1)}x^2\right) \tag{C-11}$$

where

$$x = \frac{B_o}{B_1} = \frac{\rho_o}{\rho_1} \tag{C-12}$$

For reqular gas dynamics the equation reduces to the left-hand side of C-11. For $M_o \rightarrow \infty$,

$$x^2 - \frac{2\gamma}{\gamma + 1}x + \frac{\gamma - 1}{\gamma + 1} = 0 \tag{C-13}$$

For $\gamma = 1.4$

37

$$x = 1 \text{ Mach wave} \tag{C-14}$$

$$x = 1/6 \text{ compression wave} \tag{C-15}$$

Linearizing Eq. C-11 about $x_0 = 1/6$:

$$M_o^2 f(x) \approx -1 + 2S \tag{C-16}$$

$$x_1 \approx \frac{6}{5} \left(\frac{1 + 2S}{M_o^2} \right) \tag{C-17}$$

Requiring $x_1 \leq 1/20$

For $S \leq 10$

Eq. C-17 gives

$$M_o \geq 22 \tag{C-18}$$

Under these conditions the shock relations can be used:

$$\frac{P_y}{P_x} = \frac{2\gamma}{\gamma + 1} M_x^2 - \frac{\gamma - 1}{\gamma + 1} \tag{C-19}$$

$$\frac{T_y}{T_x} = \frac{\left(1 + \frac{\gamma - 1}{2} M_x^2 \right)\left(\frac{2\gamma}{\gamma - 1} M_x^2 - 1 \right)}{\left(\frac{(\gamma+1)^2}{2(\gamma-1)} M_x^2 \right)} \tag{C-20}$$

$$V_x^2 + \frac{2}{\gamma - 1} C^2 = \frac{\gamma + 1}{\gamma - 1} V_x V_y \tag{C-21}$$

where x and y refer to upstream and downstream conditions respectively. The Mach numbers are measured with respect to the shock front. Applying these relations to Fig. 5 with the boundary conditions

$$V_2 = V_4 \tag{C-22}$$

$$P_2 = P_4' = P_4 + \frac{B_4^2}{2\mu_o} \tag{C-23}$$

Two relations are found between the Mach numbers

$$M_B = \frac{\sqrt{2\gamma(\gamma-1)}}{(\gamma+1)} M_a \left[\frac{1}{M_c} - M_c \right] + M_a \tag{C-24}$$

$$M_B^2 = \frac{M_a^2 \left[1 + \frac{2\gamma}{\gamma+1}(M_c^2 - 1) \right]}{\left(1 + \frac{P_B}{P_o} \right)} \tag{C-25}$$

where

$$M_a = \frac{V_a}{C_o}, \quad M_B = \frac{V_B}{C_o}, \quad M_c = \frac{V_1 + V_c}{C_1} \tag{C-26}$$

and

$$P_B = \frac{B_o^2}{2\mu_o} \tag{C-27}$$

Combining Eq. C-23 and C-24 to eliminate M_B

$$\frac{(\gamma+1) + 2\gamma(M_c^2 - 1)}{\left(1 + \frac{P_B}{P_o} \right)} = \frac{2\gamma(\gamma-1)}{(\gamma+1)} \left[\frac{1}{M_c} - M_c \right]^2 + (\gamma+1) + 2 \left[\frac{1}{M_c} - M_c \right] \sqrt{2\gamma(\gamma-1)} \tag{C-28}$$

Assuming $M_c > 3$, Eq. C-27 reduces to a quadratic

$$M_c^2 - \frac{M_c \, 2\sqrt{2\gamma(\gamma-1)} \, (\gamma+1) \left(1 + \frac{P_B}{P_o} \right)}{2\gamma(\gamma-1)\left(1 + \frac{P_B}{P_o} \right) - 2\gamma(\gamma+1)} + \frac{(\gamma+1)^2 \frac{P_B}{P_o}}{2\gamma(\gamma-1)\left(1 + \frac{P_B}{P_o} \right) - 2\gamma(\gamma+1)} \approx 0 \tag{C-29}$$

39

After simplifying the problem to this stage only order of magnitude calculations can be made using this equation.

BIBLIOGRAPHY

1. Burgers, J. M., "Penetration of a Shock Wave into a Magnetic Field," Magnetohydrodynamics, Lockheed Symposium, Landshoff R. K. M., ed., Standford University Press, 1957.

2. Kato, Y., "Interactions of Hydromagnetic Waves," Progress of Theoretical Physics, Vol. 21, No. 3, 1959.

3. Stekly, Z. J. J., "Magnetohydrodynamic Waves in a Transverse Magnetic Field," Ph. D. Thesis, Massachusetts Institute of Technology, 1959.

4. Lewis, A. T., "A Summary of T-Type Shock Tube Research," Internal Memorandum No. 41, Energy Conversion Group, Massachusetts Institute of Technology, 1960.

5. Spitzer, L., "Physics of Fully Ionized Gases," Interscience Tracts on Physics and Astronomy, 1956.

6. Shapiro, A. H., "The Dynamics and Thermodynamics of Compressible Fluid Flow," Ronald Press Company, Vol. 1, 1953.